Soft Matter

Soft Matter

www.rsc.org/softmatter

ROYAL SOCIETY OF CHEMISTRY

ROYAL SOCIETY OF CHEMISTRY

www.rsc.org/softmatter

Journal Name

ARTICLE

Probing the Ca²⁺-assisted π-π interaction during Ca²⁺-dependent protein folding

Petra Matyska Liskova[a,b], Radovan Fiser[a,b], Pavel Macek[a] , Josef Chmelik[a], Jan Sykora[c], Lucie Bednarova[d], Ivo Konopasek[b], Ladislav Bumba[a,]*

Protein folding is governed by a balance of non-covalent interactions, of which cation–π and π–π play important roles. Theoretical calculations revealed a strong cooperativity between cation–π involving alkali and alkaline earth metal ions and π–π interactions, but however, no experimental evidences were provided in this regard. Here, we characterized a Ca²⁺-binding self-processing module (SPM), which mediates a highly-specific Ca²⁺-dependent autocatalytic processing of iron-regulated protein FrpC secreted by the pathogenic Gram-negative bacterium *Neisseria meningitidis*. SPM undergoes a Ca²⁺-induced transition from an intrinsically unstructured conformation to the compact protein fold that is ultimately stabilized by π-π interaction between two unique tryptophan residues arranged in T-shaped orientation. Moreover, the pair of tryptophans is located in a close vicinity of a calcium-binding site, suggesting involvement of a Ca²⁺-assisted π-π interaction in stabilization of the tertiary structure of SPM. This makes SPM an excellent model for investigation of the Ca²⁺-assisted π-π interaction during Ca²⁺-induced protein folding.

Introduction

Non-covalent interactions play a key role in many chemical and biological processes. Apart from electrostatic, hydrophobic and van der Waals interactions, the π–π and cation–π interactions have emerged as forces of outstanding importance in the control of structure and function of proteins in recent years[1-7]. In general, π-interactions occur in molecules with the π-system, where π-electron density on the aromatic rings creates a permanent quadrupole moment with a partial negative charge above both aromatic faces and a partial positive charge around the periphery[8]. The π–stacking (π–π interaction) is associated with the interaction between the π-orbitals of two aromatic rings, in which either (a) the angle between the ring planes is less than 30° and the distance between the ring centroids is less than 4.4 Å (face-to-face), or (b) the angle between the ring planes is between 60° and 120° and the distance between the ring centroids is less than 7.5 Å (edge-to-face)[9-15]. Cation–π interaction is essentially of electrostatic origin and facilitates attraction of organic or inorganic (metallic) cation to the negatively charged electron cloud of π systems up to the maximum distance of 6.6 Å between the ring and the cation center[16]. While the cation–π interaction has been well established between K⁺ and benzene in gas-phase studies[17], it should be considered as prominent binding force in proteins, where the aromatic rings of amino acid residues (Trp, Tyr, Phe) interact with positives charges on chains of Lys or Arg residues[18-20], as well as with alkali (Na⁺, K⁺)[21,22], alkaline earth (Mg²⁺, Ca²⁺)[23], and transition metal (Cu²⁺)[24] ions as protein cofactors.

The cooperativity of cation-π and π-π interactions appears to play as important role in protein folding, molecular recognition and supramolecular assembly. Quantum chemistry calculations revealed that π–π interactions (usually in the range 2–4 kcal/mol) are significantly strengthened (up to 17 kcal/mol) in the presence of metal ions (M)[25]. However, the binding energies of metal ions are modulated by various factors such as the identity of the metal ion, effect of size, solvation and mode of binding. Metal ions have higher affinity toward a T-shaped (perpendicular) arrangement rather than to a parallel displaced or sandwiched orientation of two aromatic residues and the cooperative effect of M-π-π interactions are substantially enhanced with divalent cations (e.g. Ca²⁺, Mg²⁺)[26,27]. Despite significant numbers of Ca²⁺-π-π and Mg²⁺-π-π motifs identified by statistical analysis of high-resolution structures in the Protein Data Bank[28,29], the experimental approach for studying M-π-π interactions in proteins has not been established yet.

In the present work, we carried out analysis of a self-processing module (SPM), a 177-residues long polypeptide derived from the internal segment of the iron-regulated protein FrpC (Fig. 1A)[30,31].

a. *Laboratory of Molecular Biology of Bacterial Pathogens, Institute of Microbiology of the ASCR, v.v.i., Videnska 1083, 14200 Prague, Czech Republic. *E-mail: bumba@biomed.cas.cz*
b. *Department of Genetics and Microbiology, Faculty of Science, Charles University in Prague, Vinicna 5, 12843 Prague, Czech Republic*
c. *J. Heyrovsky Institute of Physical Chemistry of the ASCR, v.v.i., Dolejskova 3, 18223 Prague, Czech Republic.*
d. *Institute of Organic Chemistry and Biochemistry of the ASCR, v.v.i., Flemingovo nam. 2, 166 10 Prague, Czech Republic*
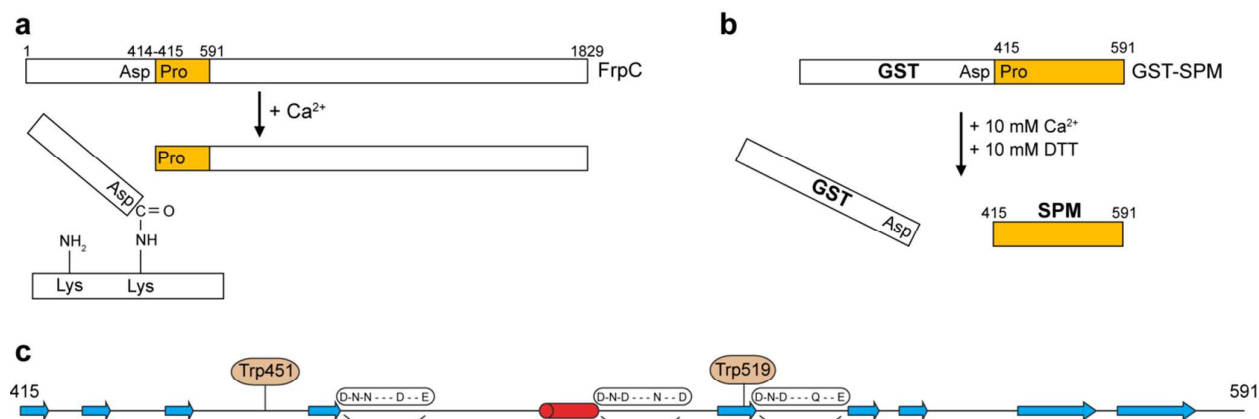
Figure 1. SPM-mediated auto-processing of the FrpC protein. (**a**) FrpC, an RTX protein secreted by the Type I secretion system of *Neisseria meningitidis*, undergoes Ca^{2+}-dependent auto-catalytic processing that is mediated by a 'self-processing module' (SPM, residues 415-591) located downstream of the cleavage site. Binding of Ca^{2+} ions promotes conformational change of SPM that results in highly specific cleavage of the Asp414-Pro415 peptide bond and covalent linkage of the generated fragment (FrpC1-414) to another protein molecule *via* a newly-formed isopeptide Asp-Lys bond. (**b**) Schematic representation of the preparation of the SPM polypeptide. Recombinant SPM was expressed in *E. coli* as the glutathione *S*-transferase (GST) fusion before the autocatalytic cleavage was induced by the addition of 10 mM Ca^{2+} ions and 10 mM dithiothreitol (DTT) to block trans-splicing activity. (**c**) Secondary structure of SPM as predicted by Jpred3[50]. α-helix and β-strands are depicted as red cylinder and blue arrows, respectively. The location of three putative calcium-binding sites is deduced on the basis of sequence homology to the 12-residue canonical EF-hand loop[48]. The residues potentially involved in calcium binding (loop sequence positions 1, 3, 5, 9 and 12) are highlighted in boxes. The position of two tryptophan residues is indicated.

FrpC is a member of the family of <u>R</u>epeat in <u>ToX</u>in (RTX) proteins characterized by C-terminal tandem repeats containing the GGXGXDXXX consensus motif[32] and secreted by the pathogenic Gram-negative bacterium *Neisseria meningitidis* during the early stages of meningococcal infection[33,34]. Although many RTX proteins serve as virulence factors secreted through the dedicated Type I Secretion System (T1SS) in Gram-negative bacteria, the biological activity of FrpC remains unknown[35]. However, FrpC undergoes autocatalytic processing that resembles "protein *trans*-splicing", a unique natural mechanism for protein editing directly at the polypeptide level. Specifically, SPM mediates a Ca^{2+}-dependent autocatalytic cleavage of the peptide bond between Asp414 and Pro415 of FrpC[30]. The resulting N-terminal fragment of FrpC (FrpC1-414) can then react through its carboxy-terminal group of Asp414 within an ε-amino group of a lysine residue of another FrpC molecule, forming a new isopeptide bond (Fig. 1a).

Despite the fact that the three-dimensional structure of SPM remains unknown at present, the SPM polypeptide constitutes an attractive model for investigation the role of Ca^{2+}-assisted π-π interaction during Ca^{2+}-induced protein folding. We show here that the Ca^{2+}-dependent folding of SPM is a highly cooperative process that consists in transition from a natively unfolded conformation to the compact protein fold. The tertiary, calcium-loaded structure of SPM is ultimately stabilized by the π-π interaction between two tryptophan residues (Trp451 and Trp519) arranged in the T-shaped orientation. Moreover, the Trp451-Trp519 pair is located in

close vicinity to a calcium-binding site, suggesting a specific Ca^{2+}-assisted π-π interaction in the tertiary structure of SPM.

Results

To characterize SPM, a polypeptide derived from residues 414 to 591 of the FrpC protein (including the Asp414-Pro415 processing site) was expressed as a fusion protein to the C terminus of glutathione *S*-transferase (GST) and purified by affinity column chromatography followed by the calcium-induced self-processing to cleave off the N-terminal GST tag (Fig. 1b). The resulting SPM protein (residues 415-591) was found to be monomeric and highly soluble (~10 mg/ml) regardless of the presence or absence of Ca^{2+} ions (Fig. S1, Supplementary Information).

π-π interaction of Trp451 and Trp519 in SPM

The analysis of the primary amino acid sequence of SPM revealed two tryptophan (Trp) residues (at positions 451 and 519 of the native FrpC protein) located within a polypeptide short of well-defined secondary structure elements (~4 % α-helix, ~28 % β-strand, see Fig. 1c). The far-UV circular dichroism (CD) spectrum of Ca^{2+}-depleted SPM showed the strong negative band at 200 nm, corresponding to an intrinsically disordered protein[36] (see Fig. 2a). The addition of 10 mM Ca^{2+} to SPM resulted in significant far-UV CD changes characterized by a bisignate CD curve with positive (230 nm) and negative (215 nm) band, respectively (Fig. 2a). The signs of these "split" Cotton effects reflect a through-space coupling of
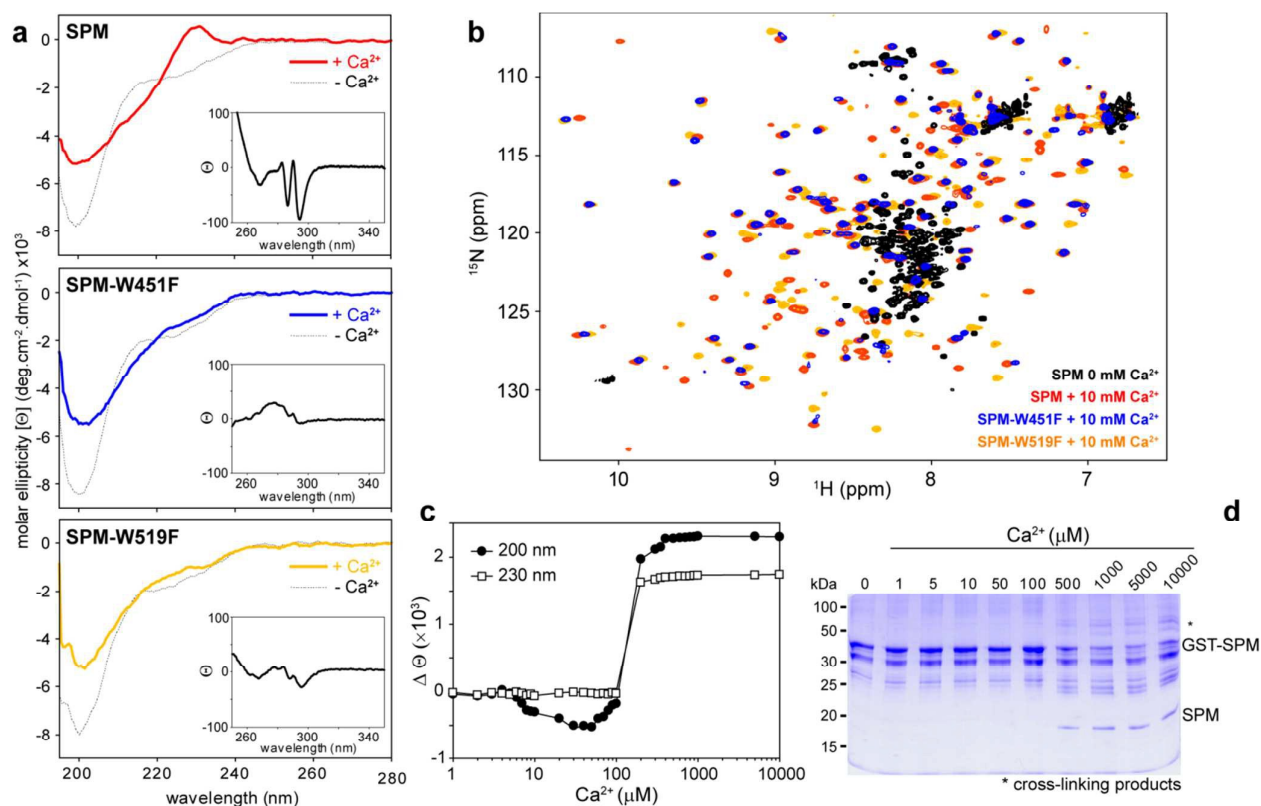
Soft Matter Accepted Manuscript

Figure 2. The Ca²⁺-dependent folding of SPM is closely associated with the auto-processing activity. (**a**) The far-UV CD spectra of the wild-type SPM (upper panel), SPM-W451F (middle panel) and SPM-W519F (lower panel) mutants in the absence (dotted thin line) and presence of 10 mM Ca²⁺ (colored thick line). (*inset*) The near-UV CD spectrum of the corresponding protein in the presence of 10 mM Ca²⁺. (**b**) Overlay of the ¹H-¹⁵N HSQC spectra of ¹⁵N-labeled SPM in the absence (black) and the presence of 10 mM Ca²⁺ (red), and the Ca²⁺-loaded SPM-W451F (blue) and SPM-W519F (orange) mutants. (**c**) Ca²⁺-induced changes in secondary (200 nm) and tertiary (230 nm) structure of SPM. SPM (5 μM) was titrated with Ca²⁺ ions and the changes in molar ellipticity were followed at 200 and 230 nm as a function of calcium concentration. (**d**) The GST-SPM fusion protein (10 μM) was incubated at the indicated concentrations of Ca²⁺ ions at 37 °C for 30 min, and the aliquots of the processed proteins were separated by 12 % SDS-PAGE gels.

electric transition moments of interacting chiral chromophores[37], indicating exciton coupling of two Trp residues. Furthermore, the near-UV CD spectrum of the Ca²⁺-loaded SPM showed two prominent negative bands at 287 and 295 nm (*inset* in the upper panel of Fig. 2*a*), which could be assigned to two negative vibronic components of ¹L_b electronic transition of tryptophan. Such ¹L_b bands have been previously shown to be characteristic for π-π interaction of two Trp residues arranged in the edge-to-face (T-shaped) orientation[38], suggesting a similar arrangement of Trp451 and Trp519 in the tertiary structure of SPM.

The specific orientation of the Trp451-Trp519 pair was examined in two SPM mutants, SPM-W451F and SPM-W519F, each carrying a single substitution of Trp to Phe residue. Both SPM mutants were prepared by the Ca²⁺-induced cleavage of the GST-SPM fusions, suggesting that neither Trp451 nor Trp519 is a catalytic residue involved in the auto-processing reaction. However, the cleavage efficacy of the SPM mutants was significantly reduced, indicating a stabilizing effect of the Trp residues (Fig. S2). The far-UV CD spectra of the SPM mutants were comparable to that of the wild-type, except that the exciton-coupled bands at 215 and 230 nm were missing in the spectra of the Ca²⁺-loaded SPM-W451F and

SPM-W519F proteins, respectively (Fig. 2a). Similarly, the distinct negative bands at 287 and 295 nm were much weaker in the near-UV CD spectra of the Ca²⁺-loaded SPM mutants (Fig. 2a, *insets*), suggesting a specific interaction of ¹L_b electronic transition dipoles between Trp451 and Trp519 side chains.

Auto-processing activity of SPM is associated with Ca²⁺-induced conformational switch from unfolded to the folded state

To shed light on the high-resolution picture of the physical state of SPM proteins, we employed nuclear magnetic resonance (NMR) spectroscopy. As illustrated in Fig. 2b, the ¹H-¹⁵N heteronuclear single-quantum coherence (HSQC) spectrum of Ca²⁺-depleted SPM showed a very narrow dispersion of chemical shifts, indicative of an unstructured protein. In contrast, the HSQC spectra of Ca²⁺-loaded SPM, SPM-W451F and SPM-W519F were characterized by a broad dispersion of backbone amide cross-peaks typical for well-folded proteins. Moreover, the dispersion of chemical shifts in the fingerprint spectra was comparable, documenting that the overall fold of SPM mutants was not affected upon Trp substitutions (Fig. 2b).

Changes in secondary structure of SPM upon calcium titration were further monitored by using the changes in molar ellipticity at 200 nm ($\Delta\Theta_{200nm}$). As shown in Fig. 2c, apparent structural changes were observed upon addition of ~10 μM Ca^{2+} followed by a distinct, highly cooperative conformational transition occurring at about 150 μM Ca^{2+}. Moreover, this Ca^{2+}-induced conformational switch was associated with formation of the exciton couplet between Trp451 and Trp519 ($\Delta\Theta_{230nm}$ in Fig. 2c) as well as the cleavage of the GST-SPM fusion protein (Fig. 2d). Collectively, these data suggested that the cleavage of the Asp-Pro peptide bond is associated with a highly cooperative, Ca^{2+}-induced conformational rearrangement from a natively-disordered to the compact protein structure that is stabilized by π-π interaction between Trp451 and Trp519 side chains.

Ca^{2+} stoichiometry for SPM

The luminescent properties of terbium (Tb^{3+}), a trivalent lanthanide possessing high affinity for calcium-binding sites in proteins, were used to probe Ca^{2+} stoichiometry for SPM. Free Tb^{3+} ions are readily quenched by water molecules, while the binding of Tb^{3+} to a protein causes a tremendous enhancement of Tb^{3+} phosphorescence with the maximum wavelength emission at 545 nm. Equilibrium titration of SPM with Tb^{3+} revealed a significant increase of phosphorescence intensity of the Tb^{3+}-SPM complex yielding a saturable binding curve (Fig. 3a). Linear extrapolation of protein binding to the theoretical maximum level of binding (dashed line in Fig. 3a) indicated that about five Tb^{3+} ions were bound to each SPM molecule. This would be a maximum stoichiometry since it is possible that some of Tb^{3+} can occupy binding sites not involved in forming a productive ligand-protein complex.

To evaluate the functional replacement of Ca^{2+} with Tb^{3+}, we tested structural and catalytic properties of SPM in the presence of Tb^{3+}. The far-UV CD spectrum of Tb^{3+}-loaded SPM were identical to that of the Ca^{2+}-loaded counterpart, documenting the structural integrity of SPM in the presence of Tb^{3+} (Fig. S3). Incubation of GST-SPM with Tb^{3+} ions resulted in a complete aggregation of the sample, probably due to oxidation of four cysteine (Cys) residues in GST[39]. On the other hand, addition of Tb^{3+} to FrpC1-862, a Cys-free construct carrying the first 862 residues of FrpC, yielded the expected 45-kDa and 42-kDa fragments along with several higher molecular weight species generated by covalent linkage of the cleaved N-terminal 42-kDa fragment to neighboring molecules (Fig. 3b). The formation of two protein fragments as well as higher molecular cross-linked products were comparable to that of mediated by Ca^{2+} ions, suggesting that both Ca^{2+} and Tb^{3+} work in concert to elicit auto-processing activity of SPM.

To further corroborate whether Tb^{3+} would compete with Ca^{2+} for the identical calcium-binding sites, the Tb^{3+}-loaded SPM was titrated with Ca^{2+} and the Tb^{3+} release was monitored by Tb^{3+} phosphorescence. As shown in Fig. 3c, Ca^{2+} titration of Tb^{3+}-loaded SPM resulted in a rapid drop of phosphorescence intensity at 545 nm, indicating displacement of Tb^{3+} by Ca^{2+} and quenching of released Tb^{3+} by surrounding water molecules. Moreover, analysis
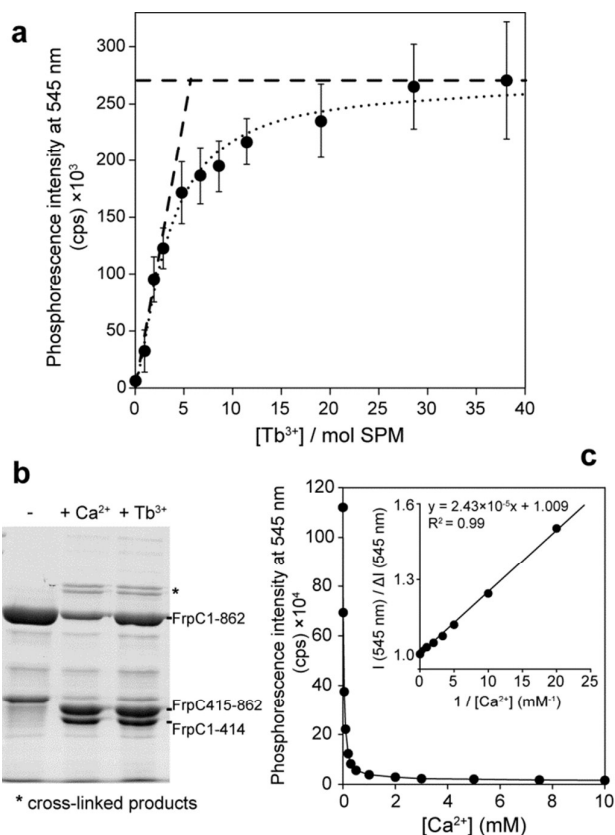

Figure 3. SPM binds five calcium ions. (**a**) Equilibrium titration of SPM with Tb^{3+}. Binding of Tb^{3+} to SPM (5 μM) was monitored as terbium phosphorescence at an emission wavelength of 545 nm after excitation at 240 nm. The dotted line represents a fit of the experimental data by Hill equation. The theoretical maximum binding is indicated by the dashed horizontal line. The number of metal ions needed for binding was determined by linear extrapolation of the binding curve to the theoretical maximum binding (the inclined dashed line). (**b**) The purified FrpC1-862 protein (2 μM) was left alone (-) or incubated in the presence of 200 μM $CaCl_2$ (+Ca^{2+}) or $TbCl_3$ (+Tb^{3+}) for 30 min at 37 °C before the protein samples were separated by 12 % SDS-PAGE gel. The cross-linked products are highlighted by *. (**c**) Tb^{3+}-loaded SPM (5 μM) was titrated with Ca^{2+} and the release of Tb^{3+} from SPM was monitored by terbium phosphorescence at 545 nm (excitation at 240 nm); Inset: linear regression of the terbium phosphorescence quenching data depicted in the modified Stern-Volmer plot. The y-axis intercept of 1.01 shows that more than 99 % of Tb^{3+} are accessible for Ca^{2+}.

of the phosphorescence quenching data by modified Stern-Volmer plot revealed that Tb^{3+} can be quantitatively outcompeted by Ca^{2+}, suggesting that SPM would bind five calcium ions.

Calcium-binding site is located in close vicinity to Trp519

The relative proximity of a calcium-binding site to Trp residue was determined from quenching experiments with Tb^{3+}. Terbium can be excited by Forster resonance energy transfer (FRET) from Trp residues and the FRET efficiency decreases with the sixth power of
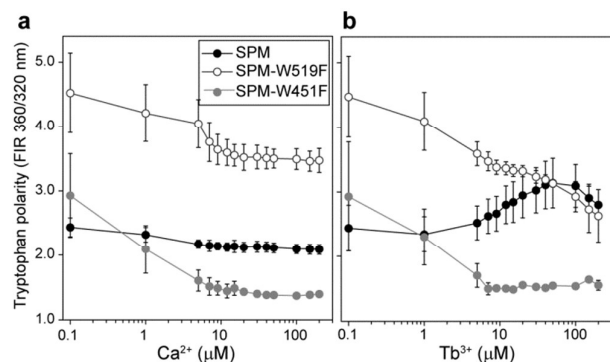
Figure 4. Distinct spectroscopic signatures of Trp451 and Trp519 in SPM. SPM, SPM-W451F and SPM-W519F (5 µM) were titrated with Ca^{2+} (**a**) or Tb^{3+} (**b**), and changes of in tryptophan polarity were followed by the ratio of fluorescence intensities emitted at 360 nm and 320 nm (FIR360/320)[40]. The values represent mean ± S.D. from three independent experiments.

the Trp-Tb^{3+} distance[40]. First, spectral properties of each Trp residue were examined upon titration experiments using Ca^{2+} and Tb^{3+} performed with the SPM-W451F and SPM-W519F mutants. Regardless of the ligand, both Trp451 (as inferred from SPM-W519F) and Trp519 (as deduced from SPM-W451F) exhibited a progressive blue-shift in the wavelengths of maximum emission (λ_{max}) from 348 to 342 nm and 340 to 329 nm, respectively. This well documented exclusion of water from the tryptophan environment and progressive exposure of tryptophan side chain into hydrophobic protein interior during Ca^{2+}/Tb^{3+}-dependent folding (Fig. S4). In parallel, polarity of single Trp residues, characterized by the ratio of fluorescence intensities emitted at 360 nm and 320 nm (FIR360/320)[41], was not affected by the ligands and the FIR360/320 values gradually decreased from 4.5 to 3.5 and from 3.0 to 1.3 for SPM-W519F and SPM-W451F, respectively (Fig. 4). These results clearly revealed that each of two Trp residues has distinct spectral properties, where Trp451 remains essentially highly exposed to the solvent, while Trp519 is associated with a highly hydrophobic interior of the folded protein.

Spectral properties of the particular Trp residues were further used to deconvolve the tryptophan fluorescence emission spectra of the wild-type SPM upon Tb^{3+} titration. As shown in Fig. 5a, each spectrum was composed of two components, each corresponding to fluorescence emission of Trp451 and Trp519 at a given Tb^{3+} concentration. Changes in fluorescence intensity of individual Trp components during the folding of SPM were expressed as relative contribution of the individual Trp components. Trp451 showed a gradual increase in the fluorescence intensities followed by a rapid drop of the intensity after 100 µM Tb^{3+}, indicating a partial quenching of Trp451 by the Tb^{3+} in the folded SPM structure (Fig. 5b). In contrast, the fluorescence intensity of Trp519 was completely quenched at 30 µM Tb^{3+}, suggesting a more complete structural stabilization of the Trp519 side chain in close vicinity to a high-affinity calcium-binding site during SPM folding.
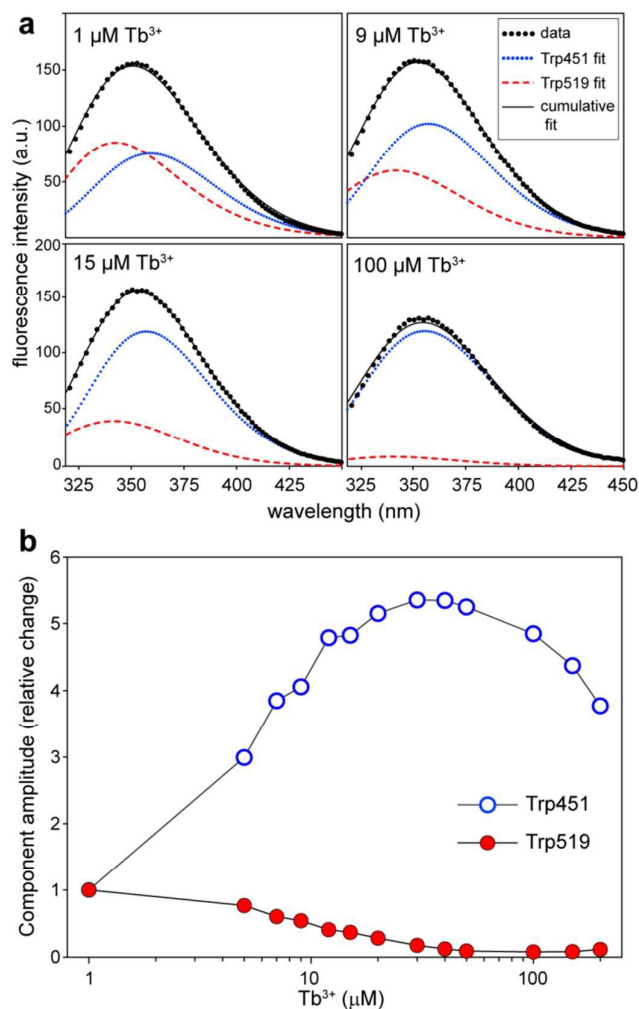

Figure 5. Deconvolution of Trp emission spectra of Tb^{3+}-titrated SPM. (a) Experimental spectra (black dots) were deconvolved into individual contributions of the Trp451 (dotted blue line) and Trp519 (dashed red line) components. λ_{max} of individual fits reflect λ_{max} of the Trp451 and Trp519 residues obtained experimentally from Tb^{3+} titration of the SPM-W519F and SPM-W451F mutants, respectively (cf. Fig. S4). Black lines represent the cumulative fit of the individual components. (**b**) Relative changes in fluorescence contribution of single tryptophan residues during titration of SPM with Tb^{3+}. The values represent fold changes in fluorescence intensity of Trp451 and Trp519 calculated on the basis of peak area integration at given Tb^{3+} concentrations.

Spatial orientation of the calcium-binding site and the Trp side chains in SPM

Spatial distribution between the calcium-binding site and tryptophan residues was determined using FRET followed by time-resolved tryptophan fluorescence spectroscopy. The energy transfer results in shortening of Trp fluorescence lifetime in the presence of the acceptor (Tb^{3+}) and the FRET efficiency was employed to measure the distance between Tb^{3+} and tryptophan. Fluorescence intensity decays of Tb^{3+}- and Ca^{2+}-loaded SPM proteins were fitted by a triple exponential decay model that provided reasonable fits (as highlighted by χ^2 and residuals in Fig.

S5). The averaged lifetimes, calculated from individual lifetime components τ_1, τ_2 and τ_3 along with their fractional contributions B1, B2 and B3, were taken to calculate the transfer efficiency and the donor-acceptor distance. As shown in Fig. S5b, such an approach was available only for SPM-W519F that exhibited shortening of the averaged lifetime of Trp451 (from 7.1 to 6.5 ns) in the presence of Tb^{3+}. On the other hand, the average lifetimes (3.7 ns) of Trp519 remained unchanged for both Ca^{2+} and Tb^{3+}-loaded proteins, indicating the absence of Tb^{3+} or, most likely, a total quenching of the non-fluorescent Trp519-Tb^{3+} complex in the SPM-W451F mutant. In contrast, the averaged lifetime of the wild-type SPM was prolonged in the presence of Tb^{3+} (from 4.0 to 5.5 ns), which further supports the results from deconvolution of the steady-state fluorescence emission spectra showing that the relative contribution of Trp519 in Tb^{3+}-loaded SPM is negligible and thus, the longer average lifetime of Trp451 (7.1 ns) prevails in the wild-type. Based on the Forster critical distance between tryptophan and Tb^{3+} of 4.1 Å[42], the distance between Trp451 and Tb^{3+} was unambiguously determined to be 5.1 Å.

Relative orientation of the coupled tryptophan residues was examined by time-resolved fluorescence anisotropy at −73 °C. Fluorescence anisotropy measures the depolarization of the fluorescence emission, which reflects molecular rotation caused by Brownian motion and/or resonance energy transfer (energy migration) between two chromophores with a different orientation. Since the rotational motion of a protein molecule is largely restricted under cryogenic conditions, the fluorescence depolarization is primarily given by homo-FRET, which further enables the determination of the distance and angle between two tryptophan residues. Analysis of the fluorescence anisotropy decays revealed the rotational correlation time of about 0.5 ns, which corresponds to a residual motion of the indole groups (Fig. S6) However, the anisotropy decay of poly-L-Trp was stabilized at a limiting anisotropy value of $r\infty$=−0.04 indicating a highly depolarized system due to energy transfer among randomly oriented tryptophan residues. In contrast, both SPM-W451F and SPM-W519F reached the limiting anisotropy value of $r\infty$=0.18, which rather reflects the degree of orientational constraint with a semicone angle of 37 °, since no Trp-Trp energy transfer is available in single tryptophan proteins. Thus, the decrease of limiting anisotropy of the wild-type SPM to a value of $r\infty$=0.14 was considered to be a combination of depolarization via residual motion and resonance energy transfer between Trp451 and Trp519 maintaining an average angle and distance between their transition dipoles from 41° to 55° and 5 to 7 Å, respectively.

Discussion

We show that SPM represents an attractive model for studying the role of Ca^{2+}-assisted π-π interaction during Ca^{2+}-induced protein folding. In the absence of Ca^{2+}, SPM behaves as an intrinsically unstructured protein that cooperatively folds upon binding of five calcium ions into a compact protein fold, which is stabilized by the Ca^{2+}-assisted π-π interaction between two Trp residues (Trp451 and

Trp519) arranged in the T-shaped orientation. In parallel, the Ca^{2+}-induced folding of SPM is closely associated with the self-processing activity of SPM that results in the cleavage of the specific Asp-Pro peptide bond at the N-terminus of SPM. Hence, the cleavage of the Asp-Pro peptide bond makes SPM a measurable readout for the analysis of Ca^{2+}-π-π interaction.

Even though the atomic structure of SPM remains to be determined, mutual orientation of the tryptophan residues and calcium ion within the tertiary structure of SPM could be deduced from a series of spectroscopic measurements. The far-UV CD spectrum of Ca^{2+}-loaded SPM revealed a distinct couplet of positive (230 nm) and negative (215 nm) bands indicating exciton coupling between neighboring Trp residues[43,44]. Single substitutions of each of two Trp residues to Phe (W451F and W519F) resulted in the disappearance of the exciton couplet from the far-UV CD spectra of Ca^{2+}-loaded SPM mutants thereby confirming a close interaction of the Trp451 and Trp519 indole side chains in the tertiary structure of SPM (Fig. 2a). The near UV CD spectrum of the Ca^{2+}-loaded SPM revealed two prominent negative bands at 287 and 295 nm, which is a typical feature of a pair of tryptophan indole rings arranged in T-shaped orientation[37]. Moreover, analysis of tryptophan homo-FRET revealed that the distance and angle between ^1L_a-^1L_a transition dipoles of the Trp451-Trp519 pair in SPM ranges from 5 to 7 Å and 41° to 55°, respectively. Thus, the mutual orientation of two indole rings in SPM appears to be very close to that observed in tryptophan zippers (Trpzip)[37]. Trpzip is a set of well-folded 12- and 16-residue peptides that exhibit an unusually exceptional stability (ΔG_{unf}=0.6-1.7 kcal·mol^{-1} at 25 °C) comparable to much larger protein domains. High-resolution NMR structure of Trpzip revealed well-defined β-hairpin structures, which are stabilized by two pairs of Trp residues arranged in T-shaped orientation (5.5 Å, 53-72°). Such arrangement of two interacting Trp residues has been previously shown to be more favored than a face-centred parallel stack[20,45-47] and significantly contributes to stability of protein structures. This goes well with the fact that the capacity of SPM to mediate the Ca^{2+}-dependent autocatalytic cleavage of the Asp-Pro peptide bond was significantly reduced after single substitutions of each of two Trp residues, indicating the stabilizing role of π-π interaction between the Trp451 and Trp519 indole side chains (Fig. S2).

The self-processing activity of SPM is closely related to its folding that involves structural transition from a natively unfolded conformation to the compact protein fold upon binding of five calcium ions (Fig. 3a). Although the position of calcium ions in SPM remains unknown, at least three putative Ca^{2+}-binding sequences (462-474, 499–511 and 521–533) have been predicted in SPM (Fig. 1c). These sequences exhibit high homology to a 12-residue canonical EF-hand loop, in which Ca^{2+} is coordinated via side-chain carboxyl (Glu or Asp) and carbonyl (Gln or Asn) groups in the conserved position 1, 3, 5, 9 and 12 of the EF-hand motif[48]. CD titration data revealed that the Ca^{2+}-induced folding is associated with certain conformational changes (K_d ~5 μM Ca^{2+}) followed by a distinct structural rearrangement occurring at ~150 μM Ca^{2+} concentrations (Fig. 2b). Since intrinsic calcium binding affinity of
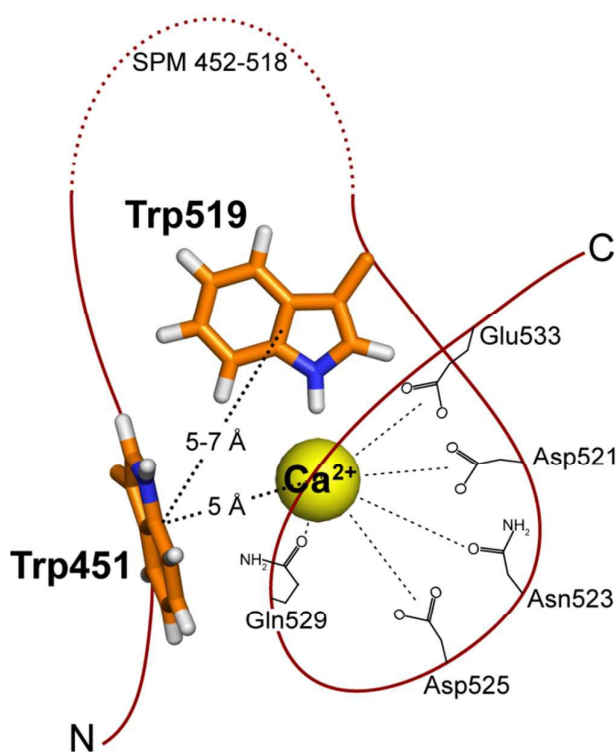
ARTICLE

Figure 6. The model of Ca^{2+}-assisted π-π interaction in SPM. The Ca^{2+} ion (yellow ball) is coordinated by ligands within a calcium-binding loop constituted by the specific sequence (SPM 521-533) homologous to the 12-residue canonical EF-hand loop. The loop binds Ca^{2+} via carboxyl and carbonyl side chains in position 1 (Asp521), 3 (Asn523), 5 (Asp525), 9 (Gln 529) and 12 (Glu533). Trp519, situated a single amino acid upstream of the loop, binds Ca^{2+} in cation–σ fashion (along the axis of the indole ring). The adjacent side chain of Trp451 is oriented perpendicularly to Trp519 and shares the identical Ca^{2+} in cation-π type of interaction. The distances (in Å) correspond to the measured values from the experimental data. The polypeptide backbone is schematically depicted as brown line with the emphasis on N and C terminus of SPM. The carbon, nitrogen and hydrogen atoms of the Trp side chains are in orange, blue, and gray color, respectively.

typical EF hands ranges from 10^{-7} to 10^{-5} M, we assume that the former structural transition (5×10^{-6} M) corresponds to local assembly of three EF hand-like loops while the rest of the polypeptide remains unstructured. The lower-affinity binding (1.5×10^{-4} M) of two additional calcium ions then induces a highly cooperative conformational switch from unstructured to the folded state, which enables the cleavage of the Asp-Pro peptide bond.

By combination of data from CD, tryptophan anisotropy and tryptophan fluorescence measurements of Tb^{3+}-titrated SPM proteins, specific arrangement of Ca^{2+} within the putative calcium binding loop 521–533 would be proposed (Fig. 6). Ca^{2+} appears to be coordinated by the side chains of five residues in the conserved position 1 (Asp521), 3 (Asn523), 5 (Asp525), 9 (Gln 529) and 12 (Glu533) of the EF-hand motif. Trp519, situated a single amino acid upstream of the putative 521-533 calcium-binding sequence,

remains closely associated with the Ca^{2+}-binding site because of a near complete quenching of its fluorescence by Tb^{3+} (Fig. 5b). In view of the fact that the side chains of Trp519 and Trp451 are oriented perpendicularly to each other within the distance of 5-7 Å, one might envisage a specific metal ion-assisted π-π interaction between the Ca^{2+} ion and the Trp451-Trp519 pair. Assuming that the Ca^{2+} ion is oriented towards Trp519 along the axis of the indole ring (cation–σ) involving a strong and short-ranged interaction (probably via the N-H group of the indole ring), then the identical Ca^{2+} ion lies perpendicularly to the adjacent indole ring of Trp451 in a cation-π fashion. Moreover, the measured distance of about 5 Å between Trp451 and Tb^{3+} is associated with similar ranges (4-6 Å) previously observed for other Ca^{2+}-π interactions[49].

Cooperativity of M-π (where M=Li^+, K^+, Na^+, Mg^{2+}, and Ca^{2+}) and π-π interactions play a major role in determining the structures of biomolecules. Statistical analysis performed on a number of three-dimensional structures taken from the Cambridge Structural Database (CSD) and Protein Data Bank (PDB) has demonstrated the presence of significant numbers of Ca^{2+}-π-π and Mg^{2+}-π-π motifs[28], even if not all of them should be considered as the true M-π-π interactions due to geometrical constraints[29]. Moreover, quantum chemistry calculations have revealed that interaction energy of π-π interaction is substantially enhanced in the presence of metal ion, and especially when the metal ion has a higher charge (i.e. Ca^{2+} and Mg^{2+} in proteins)[25]. Hence, formation of Ca^{2+}-π-π interaction could play a highly stabilizing role in the catalytically-active conformation of SPM. This conclusion is also supported by the fact that both Trp residues are well conserved in homologous sequences of other RTX proteins, which also undergo the identical Ca^{2+}-induced processing of the Asp-Pro peptide bond (Fig. S7). The magnitude of Ca^{2+}-assisted π-π interaction could be quite substantial to stabilize tertiary structure of SPM devoid of secondary structure elements. Accordingly, we believe that determination of three-dimensional structure of SPM can add insights to significance of interplay between M-π and π-π interactions during protein folding.

Experimental

Cloning, expression and purification of SPM proteins

The $FrpC_{415-591}$ protein (SPM) was expressed and purified as a C-terminal glutathione *S*-transferase (GST) fusion protein prior to a self-processing cleavage induced by calcium ions. The $frpC_{415-591}$ open reading frame was amplified from the *pTYB-FrpCΔ863-1829* construct[30] by using polymerase chain reaction (PCR) with the upstream 5'-AAA<u>GCTAGC</u>CCTAGATTTGGACGGCGAC-3' and the downstream primer 5'-AAA<u>CTCGAG</u>GAAGCGGCTGTGCAGGTTG-3' containing the *Nhe*I and *Xho*I site, respectively. The PCR product (550 bp) was cut with *Nco*I and *Xho*I (New England Biolabs, Ipswich, USA) and subcloned into the *Spe*I and *Xho*I-cleaved *pET42b* vector (Novagene, Merck KGaA, Darmstadt, Germany). Next, the 1215 bp fragment corresponding to the GST-SPM were cut by the *Nde*I and *Xho*I and cloned into NdeI-XhoI-cleaved a *pET28b* modified by a double-stranded synthetic oligonucleotide sequence encoding the N-terminal double His tag

(5'-TACCACATCATCATCATCATCATTCCCGGGCCTGGCGCCACCCGCAG
TTCGGCGGCCATCATCATCATCATCATGCTAGCATGACTGGTGGACAGC
AAATGGGTCGGGATCCGAATTCGAGCTCCGTCGACAAGCTT-3')
inserted in frame between the NcoI and NdeI sites of the *pET28b*
vector. Tryptophane substitutions to phenylalanine (W451F and
W519F) were introduced by site-directed mutagenesis by using an
overlap extension PCR with a pair of PCR mutagenic primers;
5'-CCACCGGT<u>TTC</u>GTTGCTGCC-3' and
5'-GGCAGCAAC<u>GAA</u>ACCGGTGG-3' for W451F, and
5'-TGCGTGTA<u>TTC</u>CAGGATC-3' and 5'-GATCCTG<u>GAA</u>TACACGCA-3' for
W519F substitution, respectively. The constructs were confirmed by
DNA sequence analysis with ABI Prism 3130XL analyzer (Applied
Biosystems, Foster City, USA) using a Big Dye Terminator cycle
sequencing kit.

The fusion proteins were produced in *E. coli* strain BL21(λDE3)
transformed with the appropriate plasmid. Exponential 500 ml
cultures were grown in shaking incubator at 37 °C in M9 minimal
media supplemented with kanamycin (60 µg/ml). Expression of
proteins was induced by adding 1 mM IPTG at OD_{600} = 0.6-0.8 and
bacteria were grown for additional 4 h. The cells were harvested by
centrifugation, washed two times in TNE buffer (50 mM Tris-HCl,
pH 7.4, 150 mM NaCl, 5 mM EDTA), and resuspended in TN buffer
(50 mM Tris-HCl, pH 7.4, 150 mM NaCl). The cells were
disintegrated by sonication at 4 °C and the cell lyzates were
centrifuged at 20,000 *g* for 20 min and the supernatant was loaded
onto a Ni-Sepharose beads (GE Healtcare) equilibrated with
TN buffer. The column was extensively washed with TN buffer and
the GST-SPM fusion proteins were eluted with TN buffer
supplemented with 500 mM imidazole. The collected fractions were
mixed with dithiothreitol (DTT) to a final concentration of 10 mM
before the protein solution was dialyzed overnight at 4 °C in TN
buffer supplemented with 10 mM DTT and 10 mM $CaCl_2$. Addition
of calcium ions induced a self-processing activity of SPM resulting in
the cleavage of the GST-SPM fusion proteins. The SPM protein was
purified by incubation of dialysate solution in 70 °C for 15 min
before the sample was centrifuged at 5,000 *g* for 20 min. To remove
calcium ions, protein solution was incubated with 15 mM EDTA,
loaded onto a PLRP-S reverse phase column (Agilent Technologies)
in the buffer containing 50 mM triethylamine (pH 8.5) and 5%
acetonitrile, and eluted from the column by 40% acetonitrile. The
SPM protein was concentrated by rotary vacuum evaporator and
loaded onto a Superdex HR 200 gel filtration column (GE
Healthcare) equilibrated with TN buffer. The protein concentrations
were measured by a Bradford assay and the proteins were stored at
−20 °C.

Ca^{2+}-dependent processing of SPM-containing proteins

Aliquots of GST-SPM or FrpC1-862 proteins (10 µM) were
incubated with the indicated concentrations of calcium ($CaCl_2$) or
terbium ions [$Tb(NO_3)_3$] and allowed to proceed for 30 min at 37 °C
before the reaction was stopped by mixing the sample with SDS-
PAGE loading buffer containing 0.1 M Tris-HCl (pH 6.8), 2% sodium
dodecyl sulphate (SDS), 10% glycerol, 10 mM dithiothreitol (DTT)

and 0.1% bromphenol blue. The proteins were separated by 12%
SDS-PAGE gels and stained by Coomasie blue staining.

Circular dichroism (CD) spectroscopy

The CD spectra were recorded on a Jasco-815
spectropolarimeter in rectangular quartz cells of 1-mm path length.
Protein samples (5 µM) diluted in buffer containing 5 mM Tris-HCl
(pH 7.4) and 50 mM NaCl were measured at room temperature in
the spectral interval from 195 to 280 nm with scanning speed
10 nm/min and response time of 8 ms (far-UV CD spectra), and in
the spectral interval from 240 to 370 nm with scanning speed
2 nm/min and response time of 32 ms (near-UV CD spectra). For
both spectral region the standard instrument sensitivity and two
spectra accumulation were used. Calcium titration experiments
were performed by successive addition of $CaCl_2$. The spectrum of
the buffer was subtracted from the protein spectra and molar
ellipticity (Θ) was expressed in degrees square centimeter per
decimole (deg.cm^{-2}.dmol^{-1}).

Nuclear magnetic resonance

The ^{1}H-^{15}N-HSQC spectra were recorded at 30 °C on a Bruker
Avance III 600 MHz spectrometer equipped with the cryogenic
^{1}H/^{13}C/^{15}N TCI probe head (Bruker). The ^{15}N-labeled proteins were
produced in M9 minimal medium supplemented with 0.5 g/l ^{15}NH$_4$Cl
and purified as above. The protein samples (0.5 mM) were
maintained in a buffer containing 5 mM Tris-HCl, pH 8.0, 50 mM
NaCl, 0.05% NaN$_3$, 10% D$_2$O and supplemented with 10 mM $CaCl_2$ (if
required). The NMR spectra were processed using *NMRPIPE*[51] and
analyzed in *SPARKY* (Goddard, T. D. & Kneller, D. G. *SPARKY 3.115,
San Francisco, USA, University of California,* 2006).

Tb^{3+} phosphorescence measurements

Terbium phosphorescence data were collected on a
FluoroMax-3 spectrofluorimeter (Horiba). All measurements were
recorded using a quartz cell with a 3-mm path length (Hellma) and
the sample temperature was maintained at 10 °C. The Tb^{3+} emission
spectra were measured with excitation wavelength at 240 nm and
the emission intensities were recorded between 520 and 570 nm,
with the excitation and emission bandwidths of 10 nm. Second
order diffraction was suppressed by using a 400 nm long-pass filter
(3RD400LP, Omega Optical) in the emission channel. Tb^{3+} titrations
were carried out in 10 mM HEPES buffer (pH 7.4) and 50 mM NaCl
by adding the freshly-prepared aliquots of Tb(NO$_3$)$_3$ stock solutions
into protein solution with concentration of 5 µM. The resulting
spectra were corrected for the background by subtracting the
baseline spectrum of the Tb^{3+}-free protein solution in a DataMax
software (Horiba, Japan). No protein precipitation was observed
during the experiments. The intensities at 545 nm were plotted as a
function of terbium concentrations and the data were fitted by Hill
function (Fityk 0.9.8, http://fityk.nieto.pl):

$$I = [Tb^{3+}]^n / (k_D{}^n + [Tb^{3+}]^n) \qquad \text{Eq. 1}$$

where n is the Hill number of cooperativity and k_D dissociation constant, I is intensity of terbium phosphorescence and $[Tb^{3+}]$ terbium concentration.

For competition experiments, the Tb^{3+}-loaded SPM (5 μM) was titrated with the increasing concentration of $CaCl_2$ and the intensities of terbium phosphorescence at 545 nm were plotted as a function of calcium concentrations. The fraction of Tb^{3+} bound to SPM was determined by analysis of the phosphorescence quenching data using a modified Stern-Volmer equation:

$$F_0/\Delta F = 1/(f_a.K_a.[Q]) + 1/f_a \qquad \text{Eq. 2}$$

where f_a is the fraction of the original fluorescence intensity accessible to quencher, K_a is the Stern-Volmer quenching constant of this fraction, F_0 original fluorescence intensity in absence of quencher, ΔF the difference of fluorescence intensities (F_0-F). In the modified Stern-Volmer plot of $F_0/\Delta F$ vs. $1/[Q]$, the y-intercept represents the approximation of infinitely high concentration of the quencher ($1/[Q]$ = 0) and yields f_a^{-1}[40].

Tryptophan fluorescence

Steady-state fluorescence of tryptophan was collected on a FluoroMax-3 spectrofluorimeter (Horiba, Japan). The measurements were recorded using a quartz cell with a 3-mm path length (Hellma) and the sample temperature was maintained at 10 °C. Emission spectra of tryptophan were recorded with excitation wavelength at 295 nm and the intensities were scanned between 310 and 500 nm, with the excitation and emission bandwidth of 8 nm and 6 nm, respectively. The geometry of the fluorescence detection was 54.7 °. Calcium and terbium titrations were carried out in 10 mM HEPES buffer (pH 7.4), 50 mM NaCl by adding the indicated amount of $CaCl_2$ (Sigma-Aldrich) or $Tb(NO_3)_3$ (Sigma-Aldrich) from stock solutions into protein solution with concentration of 5 μM. The resulting spectra were corrected for the background by subtracting the baseline spectrum of the buffer.

Spectra deconvolution

Deconvolution of tryptophan fluorescence spectra were done in Gnuplot 4.2 (http://www.gnuplot.info). The emission spectra of the individual SPM-W451F and SPM-W519F proteins at given Tb^{3+} concentrations were fitted with in a wavenumber scale (22000 - 32000 cm^{-1}) by log-normal function:

$$\begin{cases} I(v) = I_m \cdot exp\{- \ln2/(\ln^2\rho) \cdot \ln^2((a - v)/(a - v_m))\} & (at\ v < a) \\ I(v) = 0 & (at\ v \geq a) \end{cases}$$
Eq. 3

where I is the intensity, I_m is the maximal amplitude, v_m is the position of maximal amplitude, v_+ and v_- are positions of two half-maximal amplitudes. ρ is the band asymmetry parameter: $\rho=(v_m - v_-)/(v_+ - v_m)$ and a is the function-limiting point position: $a=v_m +(\rho (v_+ - v_-))/(\rho^2-1)$. The parameters v_+ and v_- are related to v_m by:

$$v_+ = 0.831 \cdot v_m + b_+ (cm^{-1})$$

$$v_- = 1.177 \cdot v_m - b_- (cm^{-1}) \qquad \text{Eq. 4}$$

where b_+=7070 and b_-=7780. The parameters b_+ and b_- were left to oscillate at ±250 cm^{-1} to obtain optimal fit of the spectra. Next, the spectral shapes of SPM-W451F and SPM-W519F (defined by v_m, v_+ and v_-) were taken as the input parameters and used for deconvolution of the tryptophan emission spectra of the Tb^{3+}-titrated wild-type protein as described above.

Time-resolved tryptophan fluorescence

Time-resolved fluorescence measurements were performed using a time correlated single photon counting (TCSPC) IBH 5000 U equipped with a cooled Hamamatsu R3809U-50 microchannel plate photomultiplier detector. The sample was excited at 295 nm with a pulsed light emitting diode (Picoquant PLS 300, FWHM 600 ps, 5 MHz repetition rate) with vertically oriented excitation polarizer. The emission monochromator was set to 350 nm with slits of 16 nm and geometry of 54.7 °. The Glen-Taylor polarizer was placed at the excitation arm of the fluorimeter, while the sheet polarizer was used for the emission path. Fluorescence decays were collected with 10,000 counts in the peak, the time scales were 14.3 ps per channel with 8,000 channels collected. The measurements were recorded using a quartz cell with a 3-mm path length (Hellma) and the sample temperature was maintained at 10 °C. The proteins (5 μM) were measured in a buffer containing 10 mM HEPES (pH 7.4), 50 mM NaCl supplemented with 0.2 mM of either $CaCl_2$ or $Tb(NO_3)_3$.

The experimental data were fitted in a DAS5 software (IBH) using two- or three-exponential decay, the non-linear least squares method including the impulse reconvolution with the instrumental response function (IRF, fwhm ~ 600 ps), according to:

$$I(t) = B_i \sum exp\ (-t/\tau_i) \qquad \text{Eq. 5}$$

yielding lifetimes, τ_i, and corresponding amplitudes B_i.

The average lifetime ($\tau_{ave.}$) used for donor-acceptor distance determination was calculated as:

$$\tau_{ave.} = B_i.\tau_i \qquad \text{Eq. 6}$$

For donor-acceptor (Trp-Tb^{3+}) distance calculation, Förster theory was used. The efficiency of resonance transfer between Trp and Tb^{3+} were assessed as relative change of donor lifetime of in absence (τ_D) and in presence (τ_{DA}) of acceptor[52]:

$$E = 1-(\tau_{DA}/\tau_D) \qquad \text{Eq. 7}$$

Measured efficiencies E and published values of critical Förster distance for Trp and Tb^{3+} FRET pair (R_0 = 4.1Å)[53] were used for the calculation of the distance between donor and acceptor:

$$r = R_0.[(1-E)/E]^{1/6} \qquad \text{Eq. 8}$$

where r is the distance in [Å], R_0 is the critical Förster distance and E is the efficiency of resonance energy transfer.

The time-resolved fluorescence anisotropy at −73 °C

Time-resolved fluorescence anisotropy were performed as described above except an Optistat DN cryostat (Oxford Instrument, Abingdon, United Kingdom) was used to maintain the sample temperature at −73 °C. The sample was equilibrated for at least 15 minutes before collecting the data. Fluorescence decays were collected with 10,000/7,000 counts in the peak, the time scales were 14.3 ps per channel with 8,000 channels collected. Four different orientations of the emission and excitation polarizers *(vertical/vertical, vertical/horizontal, horizontal/horizontal, horizontal/vertical)* were recorded during the measurements. The SPM proteins (5 μM) were measured in a buffer containing 10 mM HEPES (pH 7.4), 50 mM NaCl, 2 mM $CaCl_2$ and 73% (v/v) glycerol. For control experiments, 2.5 mg of poly-L-Trp (15-50 kDa, Sigma-Aldrich) was dissolved in 20 μl of dimethylsulfoxide and the suspension then dissolved in 3 ml of ethylene glycol. The anisotropy decays were fitted by the non-linear least squares method including the impulse reconvolution with the instrumental response function (fwhm ~ 600 ps) using DAS5 softwere (IBH). The G-factor (G) was determined as:

$$G = <I_{hv}(t)>_t / <I_{hh}(t)>_t \qquad \text{Eq. 9}$$

where I_{hv} corresponds to the signal measured with the horizontally polarized excitation and vertically polarized emission, and I_{hh} to the excitation and emission both polarized horizontally. The decay of the time resolved anisotropy $r(t)$ was determined as follows:

$$r(t) = ((Ivv(t) − G.Ivh(t)) / ((Ivv(t) + 2.G.Ivh(t)) \qquad \text{Eq. 10}$$

and fitted with the formula:

$$r(t) = (r_0 − r_\infty).\exp(-t/\Phi) + r_\infty \qquad \text{Eq. 11}$$

where r_0 and r_∞ stand for the limiting and residual anisotropy, respectively. Parameter Φ is the rotational correlation time. The angle between transition dipoles of the Trp-Trp pair was determined using relation between fundamental anisotropy and an angle between absorption and emission dipoles:

$$r_0 = 2/5.(3.\cos^2.\beta − 1) / 2 \qquad \text{Eq. 12}$$

where r_0 is fundamental anisotropy and β is the angle between absorption and emission dipoles[39].

Acknowledgements

References

1 J. C. Ma and D. A. Dougherty, *Chem. Rev.,* 1997, **97**, 1303.
2 C. A. Hunter, K. R. Lawson, J. Perkins and C. J. Urch, *J. Chem. Soc. Perkin Trans.,* 2001, **2**, 651.
3 M. L. Waters, *Curr. Opin. Chem. Biol.,* 2002, **6**, 736.
4 P. Chakrabarti and R. Bhattacharyya, *Prog. Biophys. Mol. Biol.,* 2007, **95**, 83.
5 L. M. Salonen, M. Ellermann and F. Diederich, *Angew. Chem. Int. Ed.,* 2011, **50**, 4808.
6 C. R. Martinez and B. L. Iverson, *Chem. Sci.,* 2012, **3**, 2191.
7 A. S. Mahadevi and G. N. Sastry, *Chem. Rev.,* 2013, **113**, 2100.
8 C. A. Hunter and J. K. M. Sanders, *J. Am. Chem. Soc.*, 1990, **112**, 5525.
9 S. K. Burley and G. A. Petsko, *Science,* 1985, **229**, 23.
10 T. Blundell, J. Singh, J. Thornton, S. K. Burley and G. A. Petsko, *Science,* 1986, **234**, 1005.
11 C. A. Hunter, J. Singh and J. M. J. Thornton, *Mol. Biol.,* 1991, **218**, 837.
12 L. Broccchieri and S. Karlin, *Proc. Natl. Acad. Sci. U.S.A,* 1994, **91**, 9297.
13 U. Samanta, D. Pal and P. Chakrabarti, *Acta Crystallogr. Sect. Biol. Crystallogr.* 1999, **55**, 1421.
14 R. Chelli, F. L. Gervasio, P. Procacci and V. Schettino, *J. Am. Chem. Soc.* 2002, **124**, 6133.
15 A. V. Morozov, K. M. S. Misura, K. Tsemekhman and D. J. Baker, *Phys. Chem. B,* 2004, **108**, 8489.
16 D. A. Dougherty, *Science,* 1996, **271**, 163.
17 J. Sunner, K. Nishizawa and P. J. Kebarle, *Phys. Chem.,* 1981, **85**, 1814.
18 J. P. Gallivan and D. A. Dougherty, *Proc. Natl. Acad. Sci. U.S.A.* 1999, **96**, 9459.
19 C. D. Andrew, S. Bhattacharjee, N. Kokkoni, J. D. Hirst, G.R. Jones and A. J. Doig, *J. Am. Chem. Soc.,* 2002, **124**, 12706.
20 C. D. Tatko and M. L. Waters, *Protein Sci.,* 2003, **12**, 2443.
21 D.R. Hall, C. S. Bond, G. A. Leonard, C. I. Watt, A. Berry and W. N. Hunter, *J. Biol. Chem.,* 2002, **277**, 22018.
22 H. Huang and M. T. Rodgers, *J. Phys. Chem. A,* 2002, **106**, 4277.
23 A. S. Reddy and G. N. Sastry, *J. Phys. Chem. A,* 2005, **109**, 8903.
24 H. Yorita, K. Otomo, H. Hiramatsu, A. Toyama, T. Miura, H. Takeuchi, *J. Am. Chem. Soc.,* 2008, **130**, 15266.
25 D. Vijay and G. N. Sastry, *Chem. Phys. Lett.,* 2010, **485**, 235.
26 A. S. Reddy, D. Vijay, G. M. Sastry and G. N. Sastry, *J. Phys. Chem. B,* 2006, **110**, 2479.
27 E. A. Orabi and G. Lamoureux, *J. Chem. Theory Comput.,* 2012, **8**, 182.
28 A. S. Reddy, D. Vijay, G. M. Sastry and G. N. Sastry, *J. Phys. Chem. B,* 2006, **110**, 10206.
29 R. Chelli and P. Procacci, *J. Phys. Chem. B*, 2006, **110**, 10204.
30 R. Osicka, K. Prochazkova, M. Sulc, I. Linhartova, V. Havlicek and P. Sebo, *J. Biol. Chem.* 2004, **279**, 24944.
31 L. Sadilkova, R. Osicka, M. Sulc, I. Linhartova, P. Novak, P. Sebo, *Protein Sci.,* 2008, **17**, 1834.
32 I. Linhartova, L. Bumba, J. Masin, M. Basler, R. Osicka, J. Kamanova, K. Prochazkova, I. Adkins, J. Hejnova-Holubova, L.

Sadilkova, J. Morova and P. Sebo, *FEMS Microbiol. Rev.*, 2010, **34**, 1076.

33 M. Coureuil, O. Join-Lambert, H. Lecuyer, S. Bourdoulous, S. Marullo and X. Nassif, *Virulence,* 2012, **3**, 164.

34 M. Pizza and R. Rappuoli, *Curr. Opin. Microbiol.,* 2015, **23**, 68.

35 S. Forman, I. Linhartova, R. Osicka, X. Nassif, P. Sebo and V. Pelicic, *Infect. Immun.,* 2003, **71**, 2253.

36 V. Kuban, J. Novacek, L. Bumba and L. Zidek, *Biomol. NMR Assign.* 2015, **9**, 435

37 I. B. Grishina and R. W. Woody, *Faraday Discuss.,* 1994, **99**, 245.

38 A. G. Cochran, N. J. Skelton and M. A. Starovasnik, *Proc. Natl. Acad. Sci. U.S.A.,* 2001, **98**, 5578.

39 H. Passow, T. Clarkson and A. Rothstein, *Pharmacol. Rev.,* 1961, **13**, 185.

40 J. R. Lakowicz, Principles of Fluorescence Spectroscopy, 3$^{\text{th}}$ Edition, Springer US, 2006.

41 A. Chenal, J. C. Karst, A. C. Sotomayor Perez, A. K. Wozniak, B. Baron, P. England and D. Ladant, *Biophys. J.,* 2010, **99**, 3744.

42 R. G. Canada and D. N. Paltoo, *Biochim. Biophys. Acta Mol. Cell Res.,* 1998, **1448**, 85.

43 E. Ohmae, Y. Sasaki and K. Gekko, *J. Biochem.* 2001, **130**, 439.

44 J. M. Christie, A. S. Arvai, K. J. Baxter, M. Heilmann, A. J. Pratt A. O'Hara, S. M. Kelly, M. Hothorn, B. O. Smith, K. Hitomi, G. I. Jenkins, E. D. Getzoff, *Science,* 2012, **335**, 1492.

45 P. Hobza, H. L. Selzle and E. W. Schlag, *J. Phys. Chem.,* 1996, **100**, 18790.

46 S. Marsili, R. Chelli, V. Schettino and P. Procacci, *Phys. Chem. Chem. Phys.,* 2008, **10**, 2673.

47 M. Chourasia, G.M. Sastry and G. N. Sastry, *Int. J. Biol. Macromol.,* 2011, **48**, 540.

48 J. L. Gifford, M. P. Walsh and H. J. Vogel, *Biochem. J.*, 2007, **405**, 199.

49 A. S. Reddy, G. M. Sastry and G. N. Sastry, *Proteins,* 2007, **67**, 1179.

50 C. Cole, J. D. Barber and G. J. Barton, *Nucleic Acids Res.* 2008, **35**, W197.

51 F. Delaglio, S. Grzesiek, G. W. Vuister, G. Zhu, J. Pfeifer and A. Bax, *J. Biomol. NMR,* 1995, **6**, 277.

52 D. Toptygin, A. M. Gronenborn and L. Brand, *J. Phys. Chem. B,* 2006, **110**, 26292.

53 L. Stryer, *Annu. Rev. Biochem.,* 1978, **47**, 819.
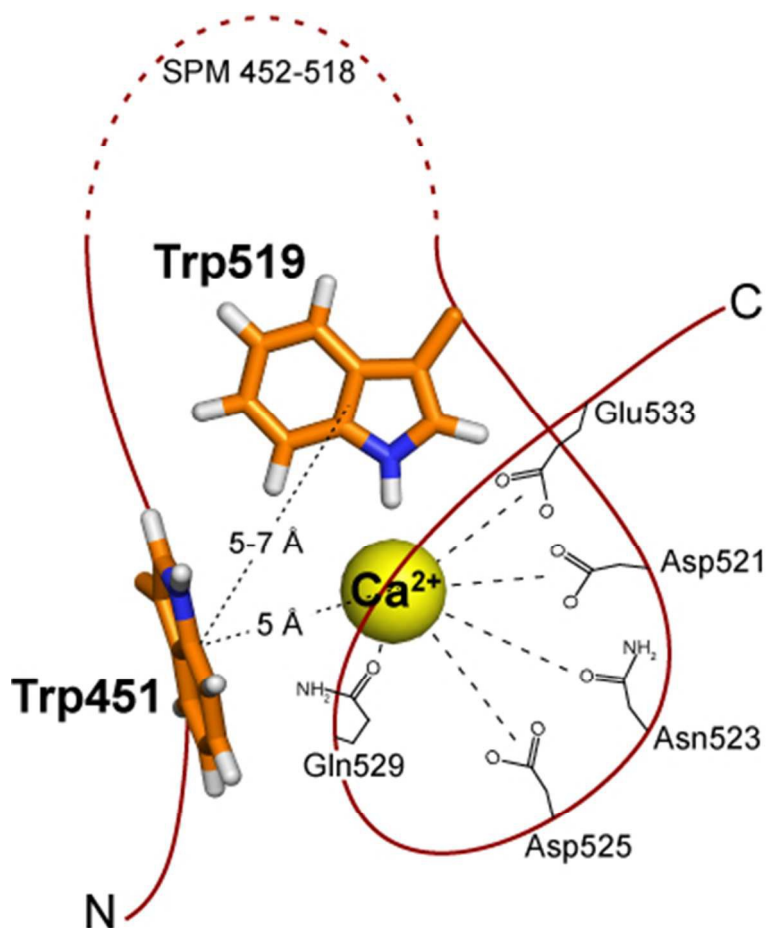
Self-processing module of the iron-regulated protein FrpC of Neisseria meningitidis serves as an excellent experimental model for investigation of the Ca2+-assisted π-π interaction during Ca2+-induced protein folding.
32x39mm (300 x 300 DPI)